IL NUOVO CIMENTO Vol. 35 C, N. 5 Settembre-Ottobre 2012
DOI 10.1393/ncc/i2012-11303-9

Communications: SIF Congress 2011

Measurement of the energy spectrum of cosmic rays using the Pierre Auger Observatory

D. Boncioli(1) for the Pierre Auger Collaboration(2)(*)

(1) *INFN and Università di Roma Tor Vergata - via della Ricerca Scientifica 1 00133 Rome, Italy*
(2) *Observatorio Pierre Auger - Av. San Martín Norte 304, 5613 Malargüe, Argentina*

ricevuto il 29 Dicembre 2011; approvato il 24 Gennaio 2012
pubblicato online il 6 Settembre 2012

Summary. — The flux of cosmic rays above 10^{18} eV has been measured with unprecedented precision at the Pierre Auger Observatory. Two analysis techniques have been used to extend the spectrum downwards from 3×10^{18} eV, with the lower energies being explored using a unique technique that exploits the hybrid strengths of the instrument. The spectral features are also presented.

PACS 98.70.Sa – Cosmic rays.
PACS 96.50.sb – Composition, energy spectra and interactions.

1. – Introduction

Ultra High Energy Cosmic Rays (UHECR) are the most energetic particles known in nature, with observed energies larger than 10^{18} eV. The detection of these particles poses many interesting questions mainly on their origin and chemical composition.

Up to now sources of UHECR are still unidentified. Magnetic fields trap particles inside the Galaxy; due to their intensity, this confinement is no longer efficient for particles with $E > 10^{18}$ eV. For these reasons, extragalactic sources need to be taken into account as candidates for UHECR production.

During the propagation from the source to the detector through astrophysical backgrounds as the cosmic microwave (CMB) and the infrared (IR) radiation fields, UHECR suffer interactions that modify their energy and nature. As an example, cosmic rays are expected to exhibit a suppression in the energy spectrum because of their interaction with CMB. This feature, known as the Greisen-Zatsepin-Kuzmin (GZK) effect [1, 2], is at about $\sim 6 \times 10^{19}$ eV for protons. It limits the horizon from which these particles can be observed to a distance below about 100 Mpc.

(*) Full author list: http://www.auger.org/archive/authors_2011_10.html

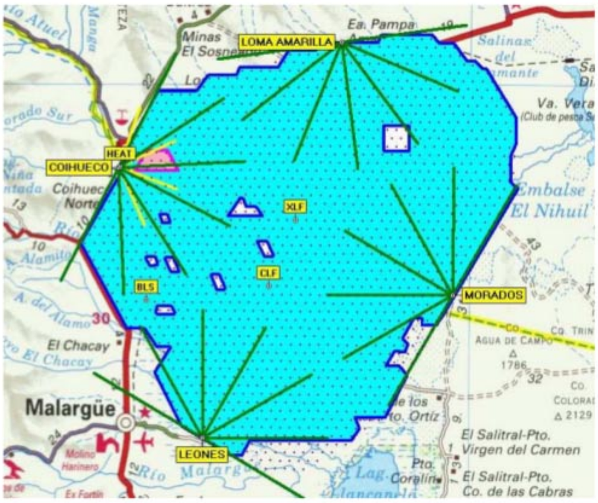

Fig. 1. – (Colour on-line) Layout of the Pierre Auger Observatory. The points indicate the surface detector stations, and the green rays indicate the field of view of each of the 24 telescopes of the fluorescence detector.

In the recent years a new step forward in unveiling the nature of UHECR was done with the measurements performed by HiRes [3] and AGASA [4] first, and nowadays with the results of the Pierre Auger Observatory [5]. The Pierre Auger Observatory measures extensive air showers (EAS) induced by the highest energy events using two complementary detection techniques: a surface detector array and a fluorescence detector. The cosmic ray flux has been measured with unprecedented precision and statistics using the Pierre Auger Observatory [6, 7].

The deviations of the energy spectrum from a constant power law have been measured, determining the position of a spectral feature (the ankle) at an energy of about 3×10^{18} eV. This break in the energy spectrum has traditionally been attributed to the transition from the galactic component of the cosmic ray flux to a flux dominated by extragalactic sources [8, 9]. In recent years it became clear that a similar feature in the cosmic ray spectrum could also result from the $e^{\pm}$ pair production process suffered by protons during propagation through CMB from extragalactic sources. In this model the transition from galactic to extragalactic cosmic rays is placed at a much lower energy [10, 11].

At energies above 4×10^{19} eV a suppression of the flux with respect to a power law extrapolation from lower energies is found, which is compatible with the predicted GZK effect, but could also be related to the maximum energy that can be reached at the sources.

In this paper we present an updated measurement of the cosmic ray energy spectrum with the Pierre Auger Observatory, as done in [7].

2. – The Pierre Auger Observatory

The Pierre Auger Observatory [5] is located near the town of Malargüe in the province of Mendoza (Argentina) at the latitude of about 35° S and altitude of 1400 above sea level. The Observatory is a hybrid system, a combination of a large surface array and a fluorescence detector (see fig. 1). The surface detector (SD) [12] is a large array of 1600 water Cherenkov counters spaced 1.5 km apart and covering a total area of 3000 km^2. Each counter is a plastic tank of cylindrical shape with size $10\,m^2 \times 1.2\,m$ filled with purified water and properly instrumented. When a UHECR particle hits the atmosphere a shower of secondary particles (mostly electrons, photons and muons) is produced. The SD tanks activated by the event record the particle number and the time of arrival. From the times, the direction of each event is determined with an accuracy of about 1°. The fluorescence detector (FD) [13] consists of 24 telescopes located in four stations which are built on the top of small elevations on the perimeter of the site. The telescopes measure the shower development in the air by observing the fluorescence light emitted in the development of the shower in the atmosphere. Each telescope has a 12 m^2 spherical mirror with curvature radius of 3.4 m and a camera with 440 photomultipliers. The field of view of each telescope is $30° \times 30°$.

The original fluorescence detector has been extended by three High Elevation Auger Telescopes (HEAT) [14]. The design of HEAT is very similar to the original FD system, except for the ability to tilt the telescopes upwards by 29°. With the HEAT enclosures in the tilted position, the combined HEAT-FD telescopes cover an elevation range from the horizon to 58°. This extended field of view enables the reconstruction of low-energy showers for close-by shower events.

The Pierre Auger Observatory is currently being enhanced with the AMIGA detector (Auger Muons and Infill for the Ground Array) to bring the energy threshold down to 10^{17} eV and to enable the muon content of air showers to be determined. AMIGA consists of an array of water-Cherenkov detectors set out on a hexagonal spacing with sides of 750 m (infill) and an associated set of muon detectors [15]. The deployment of the SD infill component started in 2008 and more than 85% of the 750 m array has already been deployed. A first analysis of cosmic rays observed with this array is presented in [16].

3. – Event reconstruction and energy calibration

The SD measures the lateral distribution of particles on ground. These signals are converted into units of vertical-equivalent muons (VEM)([1]) which are used in any further analysis of SD data. The EAS axis is obtained from the arrival time of the first particles in each detector station. The core and the lateral distribution function (LDF) are inferred from a global minimization. In general the energy of the primary particle is a function of the number of secondary particles detected at the surface, and is better correlated with the signal at a fixed distance from the core of the EAS [17]. In this case, the signal at 1000 m from the axis, $S(1000)$, corrected for the attenuation in the atmosphere, is used as an energy estimator. At this distance, the fluctuations of the signal, due to an imperfect knowledge of the LDF, are minimized [18].

The Fluorescence Detector aims to reconstruct the longitudinal development of the light emitted by the shower. The measurement is calorimetric since the energy of the primary is in principle proportional to the integral of the light along the profile. The FD is only active during clear, moonless nights.

A measurement of the development profile of the air shower (deposited energy *versus* slant depth) is possible with EAS viewed with the FD in coincidence with the SD. An example is given in fig. 2. The first step is the determination of the geometry of the axis

([1]) One VEM is defined as the average of the signals produced in the 3 PMTs of a water-Cherenkov detector by a vertical muon that passes centrally through it.

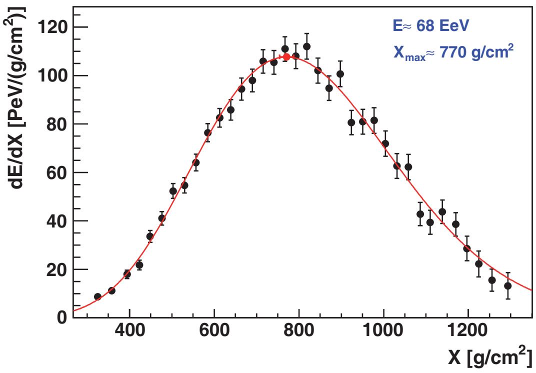

Fig. 2. – Example of longitudinal profile of high-energy shower as measured by the FD. The energy deposited by the particles of the shower is plotted as a function of the atmospheric slant depth [19].

of the EAS using directions and timing information from the FD pixels, coupled with the arrival time of the shower at the SD station with the highest signal. The procedure results in an arrival direction resolution of better than 1°. Next, the light collected in the cameras of FD is transformed into the energy deposited along the axis of the shower [20], by taking into account the fluorescence and Cherenkov light contributions and the attenuation of this light by scattering in the atmosphere. The fluorescence light emitted around 337 nm along the track of the EAS is converted into energy deposit by using the absolute fluorescence yield in air in the 337 nm band of (5.05 ± 0.71) photons/MeV of energy deposited [21], taking also into account the wavelength, temperature, pressure and humidity dependence [22]. Due to the limited field of view of the FD, the longitudinal profile is not in general recorded in its entirety, so a fit with a Gaisser-Hillas function is employed to obtain the full profile. This energy deposit profile is integrated to yield the calorimetric energy, with a correction of about 9% added to take account of the energy carried by high energy muons and neutrinos. This non-detected energy, that is the *invisible energy*, is accounted for by correcting the calorimetric energy $E_{\rm cal}$, detected by the FD. The factor $f_{\rm inv}$ is determined from simulations to obtain the total shower energy $E_{\rm FD} = (1 + f_{\rm inv})E_{\rm cal}$. It depends on the hadronic interaction assumptions and is also subject to shower-to-shower fluctuations [23]. The dependence of the energy scale on the hadronic interaction model is below 4%.

The sub-sample of EAS that are reconstructed by both the FD and the SD, called *golden hybrid events*, is used to relate the energy reconstructed with the FD, $E_{\rm FD}$, to $S(1000)$. The energy scale inferred from this data sample is applied to all showers detected by the SD array. A subset of high-quality golden hybrid events detected between 1 January 2004 and 30 September 2010 is used in the analysis of [19] to perform the energy calibration.

For a given energy, the value of $S(1000)$ decreases with the zenith angle, θ, due to the attenuation of the shower particles and geometrical effects. Assuming an isotropic flux of primary cosmic rays, we extract the shape of the attenuation curve from the data using the constant intensity cut method [24]. The attenuation curve has been fitted in [19] with a second degree polynomial in $x = \cos^2\theta - \cos^2\bar{\theta}$: $\mathrm{CIC}(\theta) = 1 + a\,x + b\,x^2$, where $a = (0.87 \pm 0.04)$ and $b = (-1.49 \pm 0.20)$. The attenuation curve is shown in

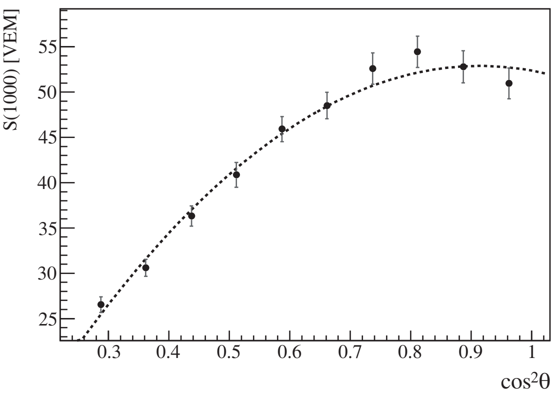

Fig. 3. – Attenuation curve, CIC(θ) fitted with a second degree polynomial in $x = \cos^2\theta - \cos^2\bar{\theta}$ [19].

fig. 3. The average angle, $\bar{\theta} \simeq 38°$, is taken as a reference to convert $S(1000)$ to $S_{38} \equiv S(1000)/\mathrm{CIC}(\theta)$. S_{38} may be regarded as the signal $S(1000)$ the shower would have produced if it had arrived at $\theta = 38°$.

The reconstruction accuracy $\sigma_{S(1000)}$ of $S(1000)$ is composed of three contributions: a statistical uncertainty due to the finite number of particles intercepted by a given SD station and the limited dynamic range of the signal detection; a systematic uncertainty due to assumptions on the shape of the lateral distribution function; and an uncertainty due to shower-to-shower fluctuations [25]. The last term contributes a factor of about 10%, while the contribution of the first two terms depends on energy and varies from 20%.

The FD energy resolution is determined by propagating the statistical uncertainty on the light flux, the invisible energy uncertainty due to shower fluctuations and the uncertainties on EAS geometry and atmospheric transparency. The overall energy resolution is 7.6% and it is almost constant with energy.

The analysis of the golden hybrid events leads to a relation between S_{38} and E_{FD}. The relation between S_{38} and E_{FD} (fig. 4) is well described by a single power-law function,

$$E_{\mathrm{FD}} = A\ S_{38}^{B}, \tag{1}$$

where the resulting parameters from the data fit are $A = (1.68 \pm 0.05) \times 10^{17}\,\mathrm{eV}$ and $B = 1.035 \pm 0.009$. The most energetic selected event has an energy of about 75 eV.

The SD energy resolution, with its statistical uncertainty, is $\sigma_E/E_{\mathrm{SD}} = (15.8 \pm 0.9)\%$ for $3\,\mathrm{EeV} < E_{\mathrm{SD}} < 6\,\mathrm{EeV}$, $\sigma_E/E_{\mathrm{SD}} = (13.0 \pm 1.0)\%$ for $6\,\mathrm{EeV} < E_{\mathrm{SD}} < 10\,\mathrm{EeV}$ and $\sigma_E/E_{\mathrm{SD}} = (12.0 \pm 1.0)\%$ for $E_{\mathrm{SD}} > 10\,\mathrm{EeV}$.

The total systematic uncertainty on the FD energy scale is about 22%. It includes contributions from the absolute fluorescence yield (14%) [21], calibration of the fluorescence telescopes (9.5%), the invisible energy correction (4%) [13], systematics in the reconstruction method used to calculate the shower longitudinal profile (10%), and atmospheric effects (6–8%) [26]. The atmospheric uncertainties include those related to the measurements of aerosol optical depth (5–7.5%), phase function (1%) and wavelength dependence (0.5%), the atmosphere variability (1%) [27] and the residual uncertainties

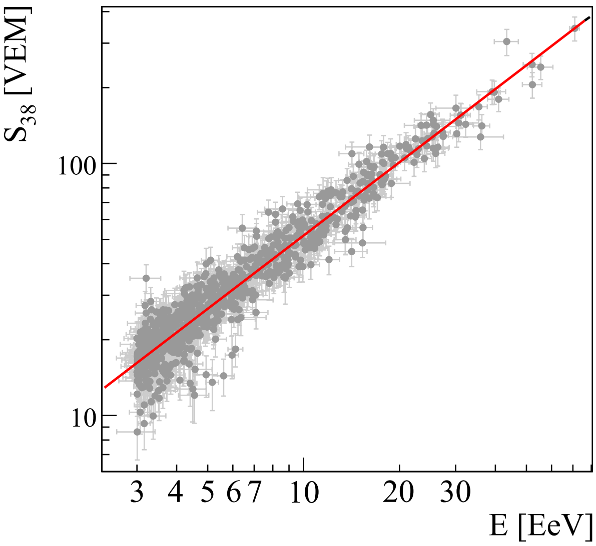

Fig. 4. – Correlation between S_{38} and E for the 839 selected hybrid events used in the fit performed in [19].

on the estimation of pressure, temperature and humidity dependence of the fluorescence yield (1.5%).

4. – The energy spectrum

Here we report the update of the energy spectrum, as given in [7], based on the surface detector data using the period between 1 January 2004 and 31 December 2010. The exposure increased by about 60% with respect to the previous publication [6] and is now 20905 km^2 sr yr. It is calculated by integrating the number of active detector stations of the surface array over time. The SD exposure is shown in fig. 5 compared to the one used in [6]. Above 3×10^{18} eV the SD acceptance is saturated regardless of the primary mass. The uncertainty on the derivation of the exposure is about 3% [28]. The event selection requires the water-Cherenkov detector with the greatest signal to be surrounded by operational stations and the reconstructed zenith angle to be smaller than 60°. The total number of events above 3×10^{18} eV fulfilling the selection criteria is about 64000. The number of events with energy greater than 10^{19} eV is about 5000.

As the energy estimator for the SD we use $S(1000)$ as explained in the previous section, together with the calibration of the energy estimator of the surface detector, whose procedure is affected by a systematic error of 22% due to the uncertainty on the fluorescence energy assignment.

The energy resolution of the SD is $\sim$ 16% at threshold, passing to $\sim$ 12% above 10 EeV, as reported in the previous section and in [19]. The influence of the bin-to-bin migration on the reconstruction of the flux due to the energy resolution has been taken into account.

The energy spectrum, including the correction of the energy resolution, is shown in the left panel of fig. 6. The number of events of the raw distribution is superimposed. The total systematic uncertainty of the flux for the derived spectrum is 6%.

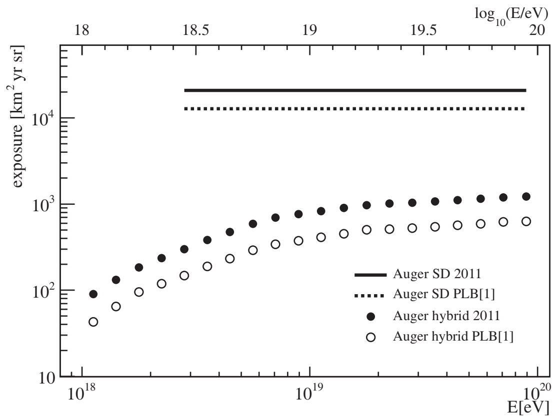

Fig. 5. – The SD and hybrid exposures used for the current flux measurement compared with a previously published data set [6]. The SD exposure is shown for energies higher than $10^{18.5}$ eV where the detector is fully efficient [7].

The energy spectrum from hybrid events is determined from data taken between 1 November 2005 and 30 September 2010. The resulting integrated exposure, presented in fig. 5 is doubled with respect to the previous publication [6,29]. To ensure good energy reconstruction only events that satisfy strict quality criteria have been accepted [29]: only showers with geometries that would allow the observation of all primaries in the range from proton to iron are retained in the data sample. A detailed simulation of the detector response has shown that for zenith angles less than 60°, every FD trigger above 10^{18} eV passing all the selection criteria is accompanied by a SD trigger of at least one station, independent of the mass or direction of the incoming primary particle [29].

The exposure of the hybrid mode of the Pierre Auger Observatory has been calculated using a time-dependent Monte Carlo simulation. The changing configurations of both fluorescence and surface detectors are taken into account for the determination of the

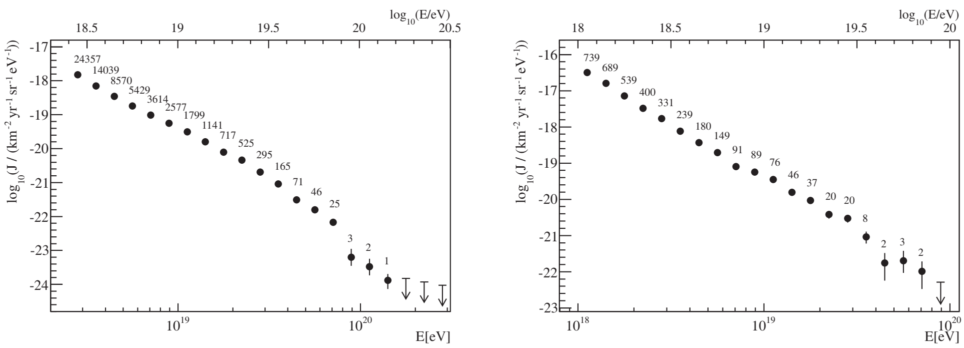

Fig. 6. – Left panel: Energy spectrum derived from surface detector data calibrated with fluorescence detector measurements. The spectrum has been corrected for the energy resolution of the detector. Only statistical uncertainties are shown. Upper limits correspond to 68% CL [7]. Right panel: Energy spectrum derived from hybrid data. Only statistical uncertainties are shown. Upper limits correspond to 68% CL [7].

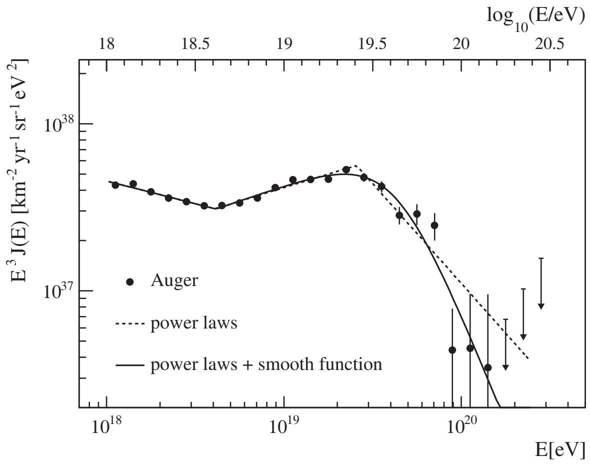

Fig. 7. – The combined energy spectrum is fitted with two functions. Only statistical uncertainties are shown. The systematic uncertainty in the energy scale is 22% [7].

on-time of the hybrid system. All atmospheric measurements [30] as well as monitoring information are also considered and used as input for the simulation. A detailed description can be found in [29, 31]. The total systematic uncertainty of the derived exposure is estimated as 10% (6%) at 10^{18} eV ($> 10^{19}$ eV).

The energy spectrum calculated using the hybrid events is shown in the right panel of fig. 6. The main systematic uncertainty is due to the energy assignment which relies on the knowledge of the fluorescence yield, choice of models and mass composition [32], absolute detector calibration [33] and shower reconstruction. The total uncertainty is estimated to be about 22%. The details can be found in [6].

The energy spectrum derived from hybrid data has been combined with the one obtained from surface detector data (see fig. 7) using a maximum-likelihood method. Since the surface detector energy estimator is calibrated with hybrid events [19], the two spectra have the same systematic uncertainty in the energy scale (22%).

The position of the ankle at $\log_{10}(E_{\text{ankle}}/\text{eV}) = 18.61 \pm 0.01$ has been determined by fitting the flux with a broken power law $E^{-\gamma}$. Two power laws in the ankle region and a smoothly changing function at higher energies have been adopted to determine the spectrum suppression by a factor two at $\log_{10}(E_{1/2}/\text{eV}) = 19.63 \pm 0.02$, where $E_{1/2}$ is the energy at which the flux has fallen to one half of the value of the power-law extrapolation. The fits are shown in fig. 7.

The suppression is similar to what is expected from the GZK effect for protons or nuclei as heavy as iron, but effects related to the acceleration mechanisms at the sources cannot be excluded.

Regarding the UHECR extragalactic propagation, a nucleon produced with an energy of 10^{21} eV beyond 100 Mpc reaches the Earth with energy lower than 10^{20} eV. In the case of cosmic ray nuclei, due to interactions with both CMB and IR photons, the nucleus can photodisintegrate; for this reason, an iron nucleus with starting energy of 10^{21} eV produced by a source beyond 100 Mpc does not reach the Earth. These different processes concerning the propagation history but involving different particles imply a steepening of the energy spectrum in the high energy region.

A suppression of the spectrum is also expected as due to the injection at the source. For instance, in the diffusive shock acceleration mechanism it is expected that a maximum energy can be attained at the source, depending on details such as the charge of the accelerated particle, the intensity of the magnetic fields and the dimensions of the accelerating region. This can be responsible for a steepening of the spectrum similar to that expected from the GZK effect.

5. – Conclusions

The cosmic ray flux has been measured with the Pierre Auger Observatory by applying two different techniques. The fluxes obtained with hybrid events and from the surface detector array are in good agreement in the overlapping energy range. A combined spectrum has been derived with high statistics covering the energy range from 10^{18} eV to above 10^{20} eV. The dominant systematic uncertainty of the spectrum stems from that of the overall energy scale, which is estimated to be 22%. The position of the ankle at $\log_{10}(E_{\mathrm{ankle}}/\mathrm{eV}) = 18.61 \pm 0.01$ has been determined by fitting the flux with a broken power law $E^{-\gamma}$. In comparison to the power law extrapolation, the spectrum is suppressed by a factor two at $\log_{10}(E_{1/2}/\mathrm{eV}) = 19.63 \pm 0.02$. The significance of the suppression is larger than 20σ.

The suppression is similar to what expected from the GZK effect for protons or nuclei as heavy as iron. The GZK cutoff could also be mimicked by acceleration cutoff at the sources; thus, a pure GZK cutoff is difficult to distinguish from a cutoff due to acceleration mechanisms.

REFERENCES

[1] Greisen K., *Phys. Rev. Lett.*, **16** (1966) 748.
[2] Zatsepin G. T. and Kuzmin V. A., *JETP Lett.*, **4** (1966) 78.
[3] Abu-Zayyad T. *et al.*, *Nucl. Instrum. Methods A*, **450** (2000) 253.
[4] Chiba N. *et al.*, *Nucl. Instrum. Methods A*, **311** (1992) 338.
[5] Abraham J. *et al.* (Pierre Auger Collaboration), *Nucl. Instrum. Methods A*, **523** (2004) 50.
[6] Abraham J. *et al.* (Pierre Auger Collaboration), *Phys. Lett. B*, **685** (2010) 239 and arXiv:1002.1975 [astro-ph.HE].
[7] Salamida F. (Pierre Auger Collaboration), *Proceedings of the 32nd ICRC, Beijing, China* (2011).
[8] Hillas A. M., *J. Phys. G*, **31** (2005) R95.
[9] Wibig T. and Wolfendale A. W., *J. Phys. G*, **31** (2005) 255 and astro-ph/0410624.
[10] Berezinsky V., Gazizov A. Z. and Grigorieva S. I., *Phys. Lett. B*, **612** (2005) 147 and astro-ph/0502550.
[11] Aloisio R., Berezinsky V., Blasi P. and Ostapchenko S., *Phys. Rev. D*, **77** (2008) 025007 and arXiv:0706.2834 [astro-ph].
[12] Allekotte I. *et al.* (Pierre Auger Collaboration), *Nucl. Instrum. Methods A*, **586** (2008) 409.
[13] Abraham J. *et al.* (Pierre Auger Collaboration), *Nucl. Instrum. Methods A*, **620** (2010) 227.
[14] Hermann-Josef Mathes T. (Pierre Auger Collaboration), *Proceedings of the 32nd ICRC, Beijing, China* (2011).
[15] Sanchez F. (Pierre Auger Collaboration), *Proceedings of the 32nd ICRC, Beijing, China* (2011).

[16] Maris I. C. (Pierre Auger Collaboration), *Proceedings of the 32nd ICRC, Beijing, China* (2011).
[17] Hillas A. M., *Acta Phys. Acad. Sci. Hung.*, **29** (1970) suppl. 3: 355.
[18] Newton D., Knapp J. and Watson A. A., *Astropart. Phys.*, **26** (2007) 414.
[19] Pesce R. (Pierre Auger Collaboration), *Proceedings of the 32nd ICRC, Beijing, China* (2011).
[20] Unger M. *et al.*, *Nucl. Instrum. Methods A*, **588** (2008) 433.
[21] Nagano M. *et al.*, *Astropart. Phys.*, **22** (2004) 235.
[22] Ave M. *et al.*, *Astropart. Phys.*, **28** (2007) 41; *Nucl. Instrum. Methods A*, **597** (2008) 46.
[23] Pierog T. *et al.*, *Czech. J. Phys.*, **56** (2006) A161.
[24] Hersil J. *et al.*, *Phys. Rev. Lett.*, **6** (1961) 22.
[25] Ave M. (Pierre Auger Collaboration), *Proceedings of the 30th ICRC, Merida, Mexico* (2007) and arXiv:0709.2125 [astro-ph].
[26] The Pierre Auger Collaboration, *Astropart. Phys.*, **33** (2010) 108.
[27] Will M. (Pierre Auger Collaboration), *Proceedings of the 32nd ICRC, Beijing, China* (2011).
[28] The Pierre Auger Collaboration, *Nucl. Instrum. Methods A*, **613** (2010) 29.
[29] The Pierre Auger Collaboration, *Astropart. Phys.*, **34** (2011) 368.
[30] Louedec K. (Pierre Auger Collaboration), *Proceedings of the 32nd ICRC, Beijing, China* (2011).
[31] Argiró S. *et al.*, *Nucl. Instrum. Methods A*, **580** (2007) 1485.
[32] Pierog T., Engel R., Heck D., Ostapchenko S. and Werner K., *Proceedings of the 30th ICRC, Merida, Mexico* (2007).
[33] Knapik R. (Pierre Auger Collaboration), *Proceedings of the 30th ICRC, Merida, Mexico* (2007).